

Surface-phonon dispersion investigation of the $(1 \times 1) \rightarrow (5 \times 1)$ reconstruction of the Ir(100) surface

S. Lehwald, J. G. Chen,* G. Kisters, E. Preuss, and H. Ibach

*Institut für Grenzflächenforschung und Vakuumphysik, Forschungszentrum Jülich,
Postfach 1913, D-5170 Jülich, Federal Republic of Germany*

(Received 9 July 1990)

High-resolution electron-energy-loss spectroscopy has been used to investigate the dispersion of surface phonons on the unreconstructed (1×1) and the reconstructed (5×1) Ir(100) surface. A significant difference in the dispersion properties of the (1×1) and (5×1) surfaces is found for both the $[011]$ and the $[001]$ direction. Lattice-dynamical calculations in a second-nearest-neighbor force-constant model fit the experimental results on the (1×1) surface if a large amount of surface stress is invoked. Our results suggest that the surface stress is the driving force for the surface reconstruction of Ir(100)- $(1 \times 1) \rightarrow$ Ir(100)- (5×1) .

I. INTRODUCTION

In the past few years high-resolution electron-energy-loss spectroscopy (EELS) has been successfully applied to measure the dispersion of surface phonons of clean and adsorbate-covered surfaces.¹⁻³ These studies have demonstrated that by comparing the experimental results with theory one is able to obtain important information concerning dynamical and structural aspects of surfaces. These studies have also revealed that the interatomic forces at the surface are in most cases different from the forces in the bulk. The capability of this method for the investigation of metastable surfaces or of surfaces with a propensity towards reconstruction is of particular importance since direct information concerning the reconstruction and relaxation mechanism is provided.

In the present study we have investigated the reconstructed and unreconstructed phases of an Ir(100) surface. It is well known from previous surface sensitive spectroscopic investigations that the Ir(100) surface undergoes a $(1 \times 1) \rightarrow (5 \times 1)$ surface reconstruction.⁴⁻⁶ What is quite unique about the Ir(100) surface is that stable and atomically clean surfaces of both Ir(100)- (1×1) and Ir(100)- (5×1) can be obtained by controlling experimental conditions. This behavior of the Ir(100) surfaces thus provides us with a unique opportunity to directly compare the properties of the surface phonons of the unreconstructed and the reconstructed surfaces. The dispersion of surface phonons has been measured along both the $\bar{\Gamma}\bar{X}$ $[011]$ and the $\bar{\Gamma}\bar{M}$ $[001]$ directions. For both directions we find that the frequency of the Rayleigh phonon near the zone boundary is higher on the (1×1) unreconstructed surface. This result is considered as being indicative of a substantial tensile stress on the (1×1) surface and that this stress plays a major role in driving the reconstruction.

II. EXPERIMENT

The experiments reported here were carried out in an ultrahigh vacuum chamber equipped with a double-pass electron-energy-loss spectrometer, low-energy electron-

diffraction (LEED) optics, an Auger-electron spectrometer (AES) and a mass spectrometer. The chamber was pumped by a 220 l/s ion pump and a liquid-nitrogen-cooled titanium sublimation pump. The base pressure of the chamber was in the low 10^{-11} mbar range.

The voltage supply of the EELS spectrometer has been described previously.⁷ In brief this computer-controlled voltage supply provided a high stability and a low noise level (<0.2 meV), which enabled us to obtain EELS spectra with a resolution [full width at half maximum (FWHM)] as good as 7.5 cm^{-1} (0.93 meV) in the elastic beam. The resolution of the EELS spectra reported here was set to be within the range of $15\text{--}25 \text{ cm}^{-1}$. The momentum-resolved EELS spectra were measured by adjusting the incident angles (θ_i) of the electron beam with fixed final scattering angles (θ_f), as described in detail previously.⁸ The impact energies of the incident electron beam used in the present study were in the range of 29–70 eV. All phonon spectra were recorded at 300 K.

The Ir(100) surface used in the present study was cut and polished to within 0.5° of the desired orientation. The crystal was initially cleaned by cycles of Ne^+ ion sputtering at 300 K ($6 \mu\text{A}$, 2 kV) for 5 min followed by annealing at 1400 K for 5 min. The final stages of cleaning involved the exposure of the crystal surface to $\sim 10 \text{ L}$ of oxygen at 1200–1300 K followed by annealing for 1 min at 1400 K. After these cleaning procedures the AES measurements revealed that the surface was free of oxygen and the impurity level of carbon was less than 1% near the surface region. The cleanliness of the surface was also assured by EELS measurements. Similar to that reported previously,⁹ the clean Ir(100) surface obtained after the above procedures was characterized by a sharp (5×1) -LEED pattern, indicating that the surface underwent a (5×1) surface reconstruction.

The preparation of a clean Ir(100)- (1×1) unreconstructed surface from an Ir(100)- (5×1) reconstructed surface has been described by other authors previously.^{5,6,10} The procedures used in the present study were as follows: A clean Ir(100)- (5×1) reconstructed surface was exposed to 45 L of O_2 at $\sim 450 \text{ K}$ followed by slowly heating the crystal to 740 K. Such a procedure resulted

in an oxygen-covered surface with an Ir(100)-(1×1)-O LEED pattern. The adsorbed oxygen was then removed by exposing the surface to 5 L of H₂ at ~525 K followed by slowly heating (~1 K/sec) to 700 K. After the above chemical treatment a clean, unreconstructed Ir(100)-(1×1) surface characterized by a sharp (1×1)-LEED pattern was routinely obtained. The surface was found to be free of oxygen as indicated by both AES and EELS measurements. Only EELS spectra with a very high magnification of about 10⁴ compared to the elastic beam indicated traces of oxygen as identified by a small vibrational loss at about 540 cm⁻¹. The carbon impurity level was less than 1% near the surface region as judged by AES measurement. Occasionally small dipole active EELS losses were observed around 125 and 195 cm⁻¹, respectively, on both clean surfaces, which were probably caused by steps or defects.

As reported previously,^{5,6,10} the unreconstructed Ir(100)-(1×1) surface was found to be stable in the temperature range of 300-700 K. Heating the Ir(100)-(1×1) surface to 1400 K gave rise to a thermally irreversible (5×1) reconstruction of the surface.

III. RESULTS

Schematic drawings depicting an unreconstructed Ir(100)-(1×1) surface and a reconstructed Ir(100)-(5×1) surface are shown in Fig. 1. These drawings are reproduced from the LEED investigations of the reconstruction of Ir(100) by Heinz *et al.*⁵ As shown in Fig. 1 the

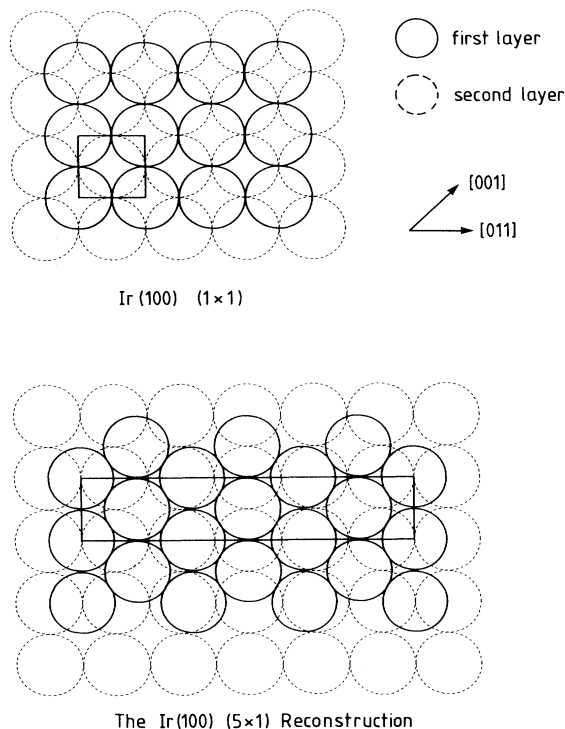


FIG. 1. Schematic drawings of the structures of Ir(100)-(1×1) and Ir(100)-(5×1). The dashed circles represent the second layer Ir atoms. The square and rectangle represent the unit cells.

unreconstructed surface is characterized by the bulk-like fourfold symmetry. LEED investigations showed that there is only a very small relaxation between the first and second surface layer of $\Delta d/d = -2\% \pm 2\%$.¹¹ The (5×1) reconstructed surface is on the other hand characterized by a quasisixfold symmetry for the top Ir overlayer. LEED analysis favored the "two-bridge" model of Fig. 1, where two of the six atoms in the (1×5) unit cell occupy precise bridge positions.⁵ The top layer is buckled so that it possesses twofold symmetry only. There are six atoms in the unit cell on five nearest-neighbor distances in [011] direction, i.e., the density of atoms in the quasihexagonal layer is 20% larger than in the (1×1) surface. Two domains, rotated by 90°, exist on the Ir(100)-(5×1) surface.

Figure 2 shows the surface Brillouin zone of an unreconstructed Ir(100)-(1×1) and a reconstructed (5×1) surface with the hexagonal overlayer considered in isolation from the substrate. In our phonon-dispersion measurements the scattering plane was aligned within ~2° along the two high symmetry $\bar{\Gamma}\bar{X}$ [011] and $\bar{\Gamma}\bar{M}$ [001] directions, respectively. For the ease of comparison the phonon spectra of the (5×1)-reconstructed surface were also measured along these two directions. By comparing Figs. 1 and 2 one can notice that the $\bar{\Gamma}\bar{X}$ [011] direction is also a high symmetry direction for the (5×1)-reconstructed surface. However, for the two domains of the overlayer, one samples two different directions in the hexagonal Brillouin zone, namely, $\bar{\Gamma}\bar{M}'$ and $\bar{\Gamma}\bar{K}'$. The $\bar{\Gamma}\bar{M}$ [001] direction is no longer a high symmetry one for the (5×1) surface, however it is unique in that it is equivalent for both domain orientations. The breakdown in the symmetry of the (5×1) surface along the [001] direction is reflected in the phonon dispersion curve, which will be presented later.

A set of phonon spectra of the unreconstructed Ir(100)-(1×1) surface measured along the $\bar{\Gamma}\bar{X}$ direction is shown in Fig. 3. The phonon wave vectors in Fig. 3 are normalized with respect to the zone boundary of the $\bar{\Gamma}\bar{X}$ direction ($Q_{\parallel} = 1.16 \text{ \AA}^{-1}$) and are represented as ξ . Figure 3(a) is a typical phonon spectrum recorded at the \bar{X}

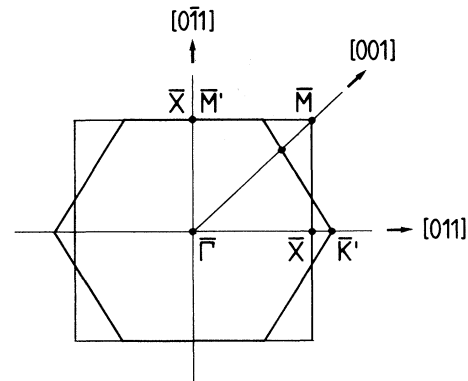


FIG. 2. Surface Brillouin zones of the unreconstructed Ir(100)-(1×1) and the reconstructed (5×1) surfaces with the hexagonal overlayer considered in isolation from the substrate. Letters with a prime refer to high symmetry points of the hexagonal Brillouin zone.

point. The peak at $\nu=0$ cm^{-1} is due to the diffuse elastic scattering of electrons with surface defects such as kinks and steps. The two inelastic peaks in Fig. 3(a) correspond to the annihilation (energy gain) and creation (energy loss) of the surface Rayleigh mode, or the so-called S_4 mode,^{12,13} respectively. As discussed previously this S_4 mode corresponds to the vertical displacement of surface layer atoms. As expected the frequency of this S_4 mode decreases at smaller wave vectors [Figs. 3(b) and 3(c)].

In principle, another surface phonon mode that corresponds to the longitudinal displacement of surface layer atoms (S_6 mode) exists close to the \bar{X} point for a fcc (100) surface.¹²⁻¹⁴ However this mode has not been detected for the Ir(100)-(1 \times 1) surface during our experiments, although an unresolved shoulder on the high-energy side of the S_4 mode was sometimes observed. We assume that under our experimental conditions the cross section for the excitation of the S_6 mode is small.

A set of phonon spectra for a (5 \times 1)-reconstructed surface along the $\bar{\Gamma}\bar{X}$ direction is shown in Fig. 4 for comparison. The first Brillouin zone of the (5 \times 1) surface ac-

tually extends only until $\zeta=0.2$ in one $\bar{\Gamma}\bar{X}$ direction, i.e., the Rayleigh mode should be folded back to yield five branches within the reduced Brillouin zone. In the course of our experiments we observed, however, in the EELS spectra no prominent loss peaks which could be assigned to backfolded branches, but we found high cross sections only for the nonbackfolded branch throughout the extended Brillouin zone. This appears to be a typical feature of systems where the reduced Brillouin zone comes about by a change in the first layer structure.¹⁵ On the other hand, backfolded branches have been observed on the reconstructed Pt(100) surface using He scattering.¹⁶ The Rayleigh mode is observed therefore as a continuous mode from $\bar{\Gamma}$ to \bar{X} and $\bar{\Gamma}$ to \bar{M} , respectively. That means the scattering cross section for processes involving a reciprocal-lattice vector of the superstructure was small for all scattering conditions we tried. We also note that the elastic intensity of the (5 \times 1) extra LEED spots was always low, when the cross section for the non-backfolded phonon branch was high.

In Fig. 4 one set of surface phonon modes is observed at 87 cm^{-1} for $\zeta=1.0$, at 77 cm^{-1} for $\zeta=0.65$, and at 50 cm^{-1} for $\zeta=0.25$, respectively. By considering the

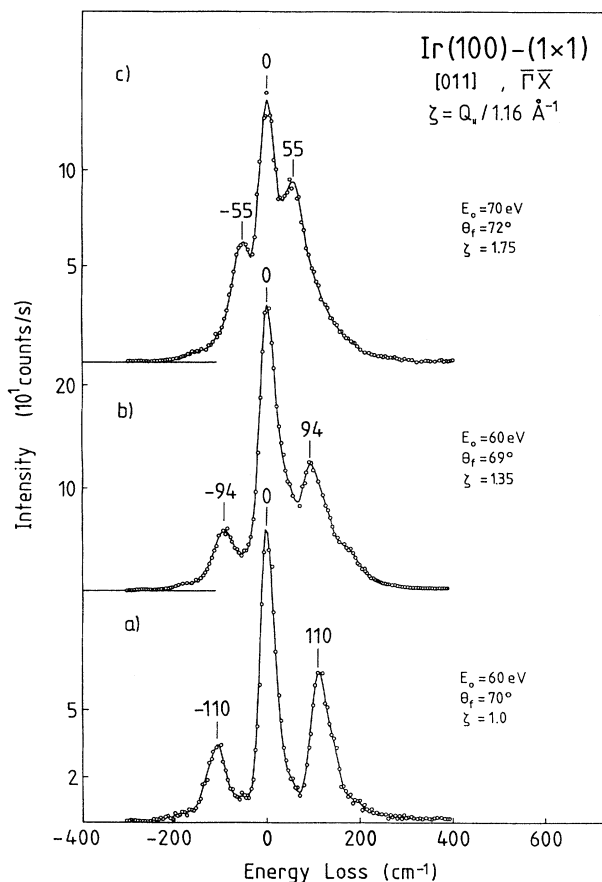


FIG. 3. Momentum-resolved EELS spectra of the unreconstructed Ir(100)-(1 \times 1) surface recorded along the $\bar{\Gamma}\bar{X}$ direction. The wave vectors are normalized with respect to the zone boundary as $\zeta=Q_{\parallel}/1.16$ \AA^{-1} . Spectra (b) and (c) are recorded within the second Brillouin zone at $\zeta=1.35$ and 1.75 , respectively.

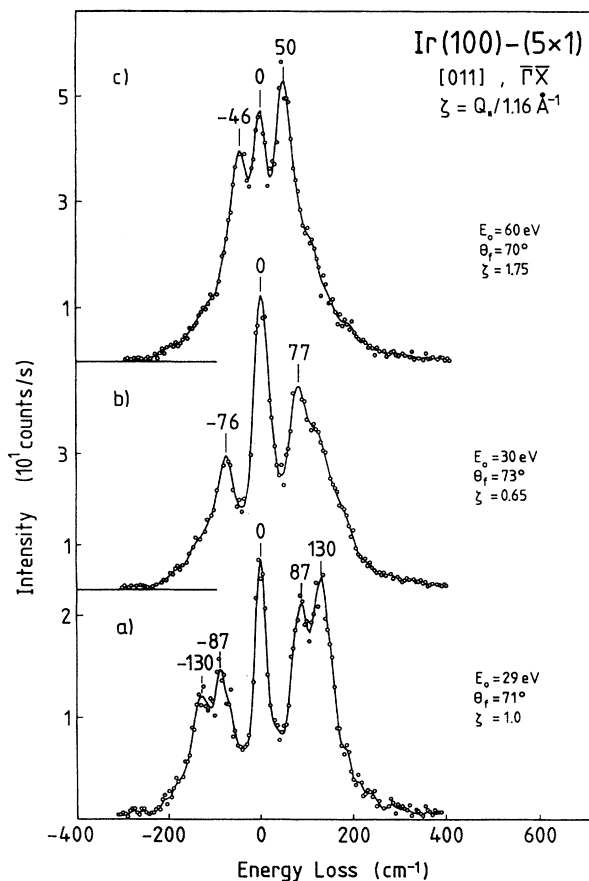


FIG. 4. Momentum-resolved EELS spectra of the reconstructed Ir(100)-(5 \times 1) surface recorded along the $\bar{\Gamma}\bar{X}$ direction. $\zeta=1.0$ corresponds to the \bar{X} point with $Q_{\parallel}=1.16$ \AA^{-1} . Spectrum (c) is recorded at $\zeta=1.75$.

quasisixfold symmetry of the (5×1) overlayer this phonon mode can be assigned to the S_1 surface mode,¹² which corresponds to the vertical displacement of the surface layer atoms. In addition to the S_1 mode, another phonon or surface resonance mode is observed at the \bar{X} point [Fig. 4(a)] at 130 cm^{-1} .

The phonon dispersion curves for the Ir(100)-(1 \times 1) and Ir(100)-(5 \times 1) surface along the $\bar{\Gamma}\bar{X}$ direction are compared in Fig. 5. A significant difference in the vibrational frequencies of the surface Rayleigh modes [S_4 for the (1 \times 1) surface and S_1 for the (5 \times 1) surface] is observed at large wave vectors. For example, at the \bar{X} point the difference in the two phonon modes is $25 \pm 2 \text{ cm}^{-1}$, indicating that the dynamical properties of the (1 \times 1) and (5 \times 1) surfaces are markedly different. Figure 5 also shows that at $\zeta < 0.4$ the phonon frequencies of these two surfaces start to overlap. This is because at long wavelength the Rayleigh wave penetrates deeply into the crystal and thus is less influenced by the first layer's structure and binding forces.

A comparison of the phonon spectra recorded at the \bar{M} point for an Ir(100)-(1 \times 1) surface and an Ir(100)-(5 \times 1) surface is shown in Fig. 6. The comparison shows again that the vibrational frequency of the surface Rayleigh mode of the (1 \times 1) surface is significantly higher than that of the (5 \times 1) surface. The difference in frequency is more clearly demonstrated in Fig. 7, where the complete phonon dispersion curves of these two surfaces are com-

pared. The pronounced difference in the phonon frequencies at $\zeta > 0.8$ confirms the difference in the dynamical properties of the two surfaces.

One should also notice from Fig. 7 that for the (5 \times 1) surface the maximum phonon frequency appears to be at $\zeta \approx 0.65$ rather than at the \bar{M} point. Such a downward curvature has been also observed for quasihexagonal (2 \times 8) and (2 \times 10) Ag overlayers on Ni and Cu(100), respectively, and has been attributed to the geometric mismatch between substrate and adlayer.¹⁵ The curvature becomes particularly large when the adlayer perpendicular vibrational mode has about the same frequency as the Rayleigh-mode. Comparing the $\bar{\Gamma}\bar{X}$ and $\bar{\Gamma}\bar{M}$ directions (Figs. 5 and 7) suggests that the effect is also related to the fact that along the $\bar{\Gamma}\bar{M}$ direction the boundary of the Brillouin zone of the hexagonal overlayer is crossed at $\zeta = 0.76$ (Fig. 2).

IV. LATTICE-DYNAMICAL ANALYSIS

The possibility for discussing the surface phonon dispersion of Ir(100) in terms of lattice-dynamical models is severely impeded by the fact that data on the bulk phonon dispersion are not available. Only the maximum bulk phonon frequency can be determined from the density of states¹⁷ to be about 6.87 THz (229 cm^{-1}). This value is consistent with the specific heat data in the regime between $\Theta_D/2$ and Θ_D , with Θ_D the Debye temperature. The knowledge of the maximum frequency is

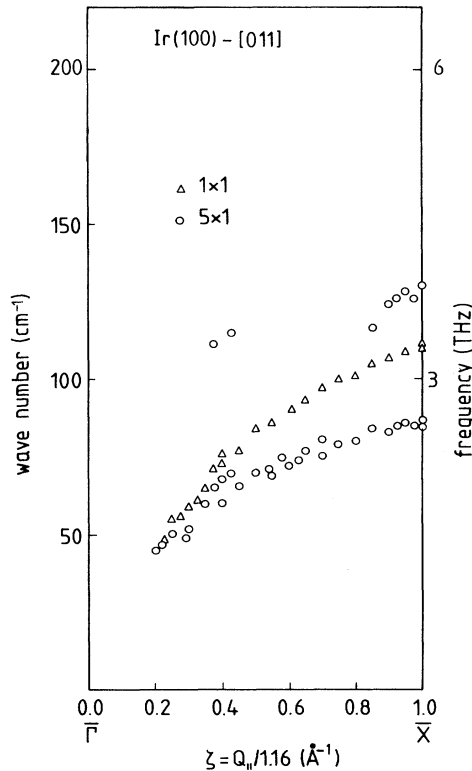


FIG. 5. Comparison of the phonon dispersion curves measured along the $\bar{\Gamma}\bar{X}$ direction for both the (1 \times 1) and (5 \times 1) surfaces.

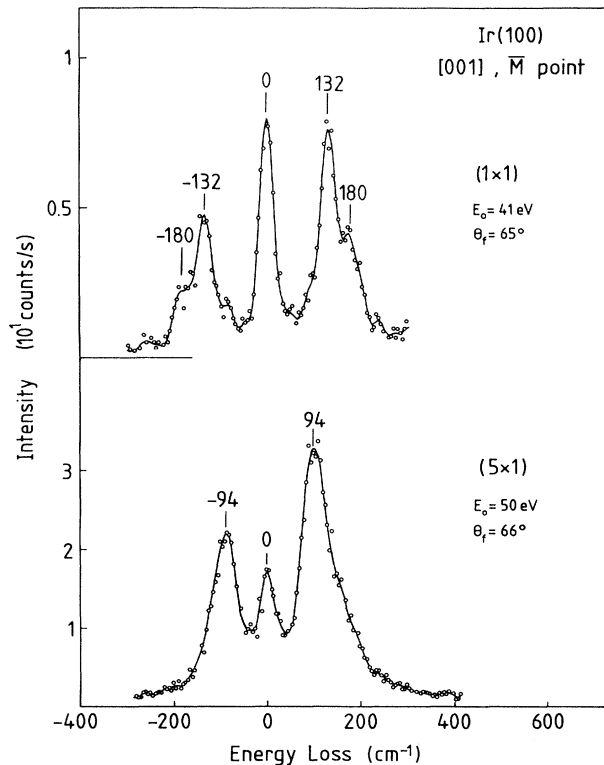


FIG. 6. Comparison of the phonon spectrum recorded at the \bar{M} point on the (1 \times 1) and (5 \times 1) surfaces, respectively.

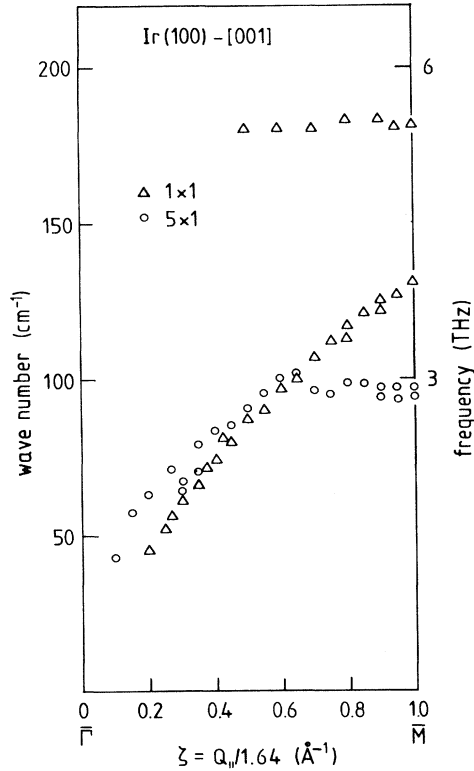


FIG. 7. Phonon dispersion curves of Ir(100)-(1×1) and Ir(100)-(5×1) measured along the $\bar{\Gamma}\bar{M}$ direction.

enough to fix the parameter of a nearest-neighbor central force model. While such a simple model fails to provide a suitable description of the elastic constants it does fit the frequencies near the boundary of the Brillouin zone for some of the 3d fcc transition metals like Cu and Ni.¹⁸

For 5d transition metals larger range interactions need to be taken into account. Also noncentral forces become important in general. For the particular case of Ir, however, the Cauchy relation between the elastic constants (here $C_{12} = C_{44}$) is well fulfilled¹⁹ and a central force constant model should therefore suffice. In order to fix the parameters for a central force constant model with second-neighbor interactions included²⁰ we have matched the parameters to provide a least-square fit to the zone boundary frequencies of platinum, an element which is next to Ir in the Periodic Table. The average deviation between the experimental frequencies²¹ and the frequencies of the model is only 1.5%. The resulting parameters were scaled to match the maximum frequency for Ir and are listed in Table I.

TABLE I. Parameters for the second-nearest-neighbor model for Ir in 10^4 dyn/cm; φ'_i and φ''_i denote the first and second derivative of the pair potential to the i th neighbor, respectively, and r_0 is the nearest-neighbor distance.

φ'_1	φ'_1/r_0	φ''_2
7.20	-0.29	0.128

The remaining parameter of the model is the first derivative of the pair potential between second-nearest neighbors φ'_2 . Its value is fixed by the condition that the bulk of the material be stress-free:

$$\sqrt{2}\varphi'_1 + \varphi'_2 = 0. \quad (1)$$

At the surface one has the additional condition that the net forces on the surface atoms must vanish. The condition is fulfilled automatically for the net force parallel to the surface by virtue of the inversion symmetry. For the perpendicular forces the condition reads for the first and second layer, respectively,

$$-u_{z1}\varphi''_2(1,3) - 4(u_{z1} - u_{z2})n_z(1,2)\varphi'_1(1,2) - \varphi''_2(1,3) + 4n_z(1,2)\varphi'_1(1,2) = 0, \quad (2)$$

$$-u_{z2}\varphi''_2(2,4) + 4(u_{z2} - u_{z3})n_z(2,3)\varphi'_1(2,3) - 4(u_{z2} - u_{z1})n_z(2,1)\varphi'_1(1,2) + 4\varphi'_1(2,3)n_z(2,3) + 4\varphi'_1(1,2)n_z(2,1) - \varphi'_2 = 0. \quad (3)$$

Here $\varphi'_i(j,k)$ and $\varphi''_i(j,k)$ denote the first and second derivative of the pair potential to the i th neighbor between layers j and k , respectively, $n_z(j,k)$ is the z component of the bond vector from an atom in the j layer to the nearest neighbor in the k layer, and u_{zj} are the vertical displacements of the atoms in the j layer; u_{z3} is assumed to be zero. If all force constants are kept at their bulk value, the surface layers relax their vertical distance. In view of the small relaxation of 2% (Ref. 11) determined by LEED we set all $u_{zj} \equiv 0$ in our model. The conditions above are then fulfilled if

$$\varphi'_1(1,2) = \frac{1}{2}\varphi'_1. \quad (4)$$

Using these parameters we have performed a lattice-dynamical slab calculation and compared the results to the experimental data. As is seen from Fig. 8 the theoretical dispersion curve runs below the experimental data near the zone boundary. Qualitatively, this result is typical for all fcc (100) surfaces (see, e.g., Ref. 13), for the Ir(100) surface, however, the difference is particularly large.

In earlier publications^{3,13,22} the surface stress mechanism has been invoked in order to explain the deviation between experimental data and the surface phonon dispersion calculated from bulk force constants. The rationale for this model is that surface atoms, by virtue of their lower coordination number, seek a smaller lateral bond distance, are however fixed in their lateral distance by the registry with the bulk lattice. In other words, surface atoms are held in a lateral distance which is larger than the equilibrium distance of their mutual pair potential. Consequently, the first derivative of the pair potential between the surface atoms $\varphi'_1(1,1)$ should shift to larger, positive values, whereas the second derivative $\varphi''_1(1,1)$ should become smaller. The picture drawn above is consistent with results from the "embedded atom" model.²³ More recently, total energy calculations have been performed for Al surfaces by Gaspar and Eguiluz.²⁴ These authors find that the primary origin for

the increased phonon frequencies is an enhanced noncentral force near the surface. At present it is not clear, however, to what extent this result bears also on transition metal surfaces with their covalent frame of d electrons. Also, in aluminum noncentral forces are large even in the bulk, as is evident from the large deviation in the Cauchy relation ($C_{12}/C_{44}=2.21$). For Ir(100) the experimental evidence is that the interlayer spacing between the first and second layer does contract by about 2%,¹¹ which is consistent with the stress model, whereas for Al(100) the interlayer spacing is expanded.^{24,25}

While the issue of whether or not noncentral forces near the surface are important for Ir(100) must await further theoretical investigations, we wish to explore here the consequences of the stress model a little further. We have calculated the surface phonon dispersion by assuming that the first derivative of the pair potential between the surface atoms $\varphi_1'(1,1)$ is positive. Figure 9 shows the comparison between the lattice-dynamical model and the experimental data for the optimum value for $\varphi_1'(1,1)/r_0=5.8 \times 10^3$ dyn/cm. Clearly, the agreement is significantly improved. A small further improvement is obtained when the second derivative of the pair potential between the surface atoms $\varphi_1''(1,1)$ is reduced. However, the data on the Rayleigh-wave dispersion are not very sensitive to that particular surface force constant. More sensitive is the S_6 mode in the gap near \bar{X} ,²⁶ which, how-

ever, was not found in this experiment.

The experimental data on the surface phonon dispersions are also crudely fitted by the lattice-dynamical model, when the force constant which couples the atoms in the first layer to the second is enhanced by about 45%. However, in view of the small contraction of the interlayer spacing by 2% there is no physical reason for such an enlargement. It was also not possible to achieve a good match to the data in both directions that way, unless more surface force constant modifications are involved. Finally an enhancement of the force constant between first and second layer by an amount larger than $\sim 30\%$ causes high-frequency surface modes to peel off the top of the phonon bulk band. Such localized high-frequency modes have however not been observed under any scattering conditions.

Figure 9 also shows the frequencies of the Rayleigh wave in the acoustic limit. The velocities of the Rayleigh wave were calculated from the elastic constants¹⁹ using the secular equations from the work of Gazis, Hermans, and Wallis.²⁷ The lattice dynamical model does not fit the acoustic limit for the Rayleigh wave properly, since longer range forces are typically necessary to account for the elastic properties. In the $\bar{\Gamma}\bar{M}$ direction the experimental data approach the Rayleigh mode in the acoustic limit, as expected. In the $\bar{\Gamma}\bar{X}$ direction however, the data cross the Rayleigh mode. This indicates that not only the

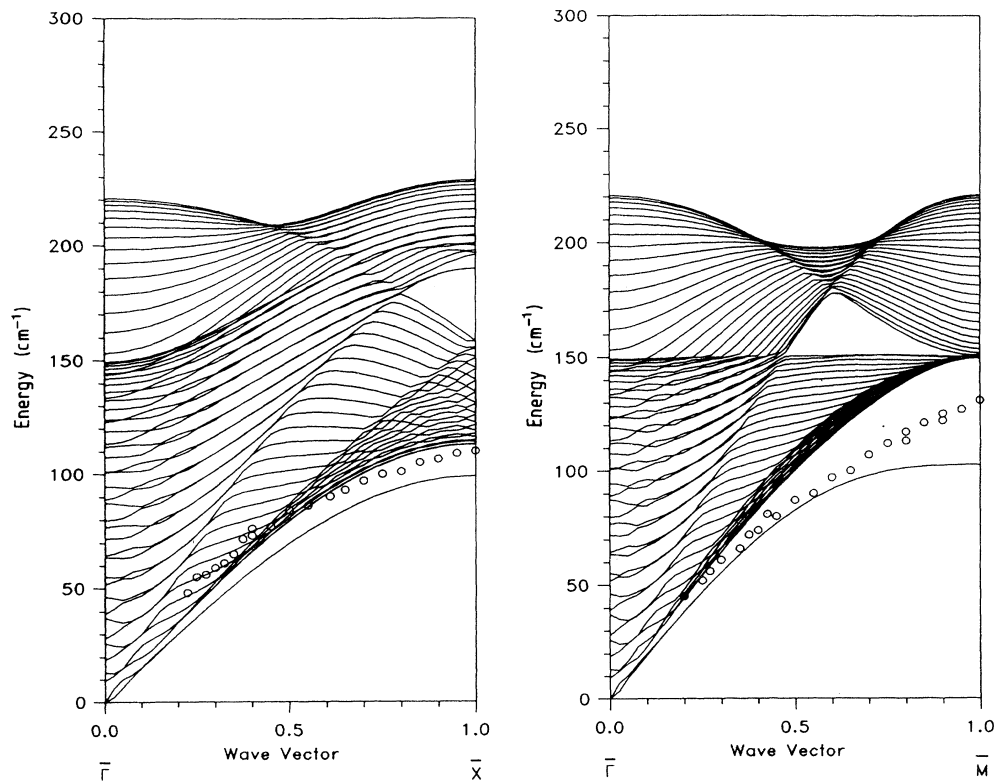


FIG. 8. Comparison of lattice-dynamical calculations (27 layers) and experimental results for the Ir(100)-(1 \times 1) surface. Only even modes are plotted. The calculations use bulk force constants of Table I and the surface equilibrium condition (4). The circles are the experimental results and are replotted from Figs. 5 and 7.

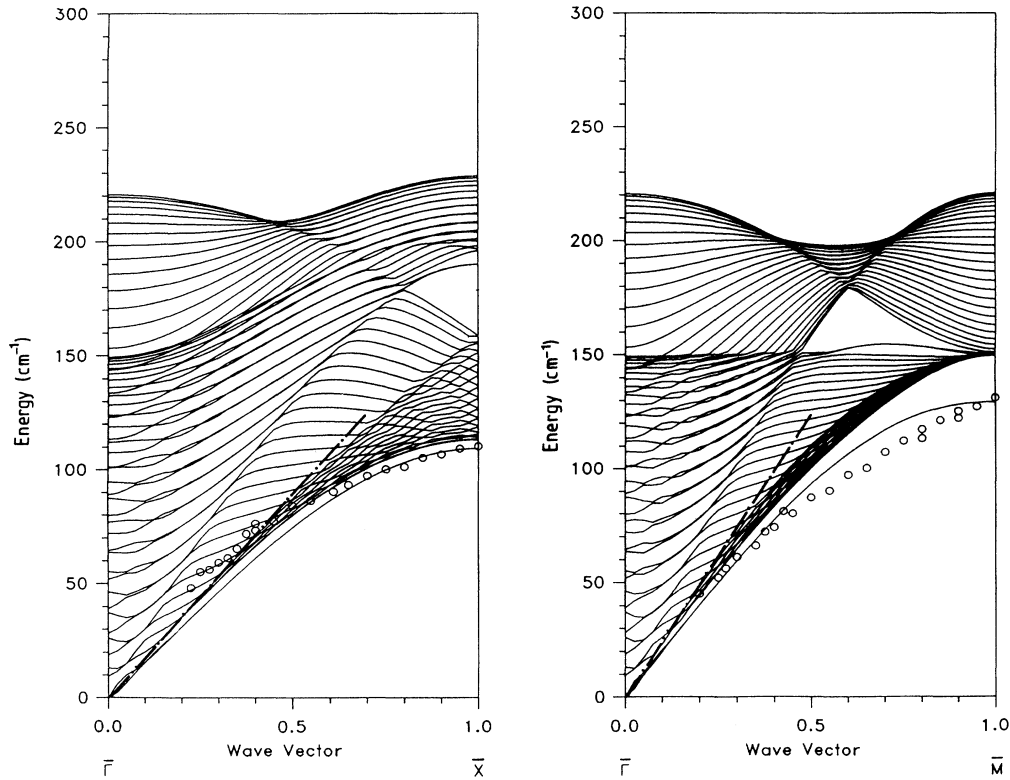


FIG. 9. The same as in Fig. 8, but with $\varphi'_1(1,1)/r_0 = 5.8 \times 10^3$ dyn/cm. The dashed-dotted line is the Rayleigh wave in the acoustic limit, as calculated from the elastic constants.

Rayleigh mode, but also the bulk band contributed to the experimental spectra. This has also been observed and confirmed by cross-section calculations on Ni(110), for example.³

V. DISCUSSION

The lattice-dynamical analysis presented above entails that the unreconstructed Ir(100) surface is under a considerably tensile surface stress. In order to estimate the amount of surface stress from the lattice-dynamical analysis it is necessary to first consider the surface stress which arises simply from the cutting of bonds alone. While conditions (2)–(4) ensure that the net forces on the surface atoms vanish, a surface stress remains and (with a_0 being the lattice constant) is equal to

$$\tau = \frac{1}{a_0} (\sqrt{2}\varphi'_1(1,1) + \sqrt{2}\varphi'_1(1,2) + 2\varphi'_2(1,1) - \frac{1}{2}\sqrt{2}\varphi'_1). \quad (5)$$

With $\varphi'_2(1,1) = -\sqrt{2}\varphi'_1$ and (4), τ becomes

$$\tau = [\varphi'_1(1,1) - 2\varphi'_1]/r_0. \quad (6)$$

Clearly, the surface is not stress-free, even when $\varphi'_1(1,1)$ is equal to the bulk value. This is a common feature of all lattice-dynamical models involving nonzero first derivatives of the pair potential and more than nearest-neighbor interactions and should be kept in mind

in the discussion of surface lattice-dynamical models.

From the fit to the dispersion curve we calculate

$$\tau \approx 1.2 \times 10^4 \quad (7)$$

in dyn/cm. This number is roughly a factor of 2 larger than the value calculated for the Ir(111) surface starting from first principles.²⁸ The surface stress found here for the Ir(100)-(1×1) surface is also by a factor of 3 to 6 larger than on the Ni(100), Ni(110), and Ni(111) surfaces.^{3,22,29} Clearly this large tensile surface stress, provided the value from the lattice-dynamical analysis is correct, must be considered as the main driving force for the reconstruction into the pseudo hexagonal overlayer. This is in agreement first with the denser packing of the first layer atoms in the (5×1) surface and second with our observation that the frequencies of the Rayleigh modes at \bar{X} and \bar{M} are significantly lower on the (5×1) than on the (1×1) surface. Thus, on the (5×1) surface the stress should be relaxed. The amount of stress energy per surface atom in the nearest-neighbor bonds may be estimated, if harmonic potentials are assumed:

$$\gamma \approx r_0^2 \tau^2 / \varphi''_1 \approx 0.92 \text{ eV}. \quad (8)$$

The (1×1)→(5×1) reconstruction proceeds via domains and islands⁵ also by producing steps so that we can assume that no additional atoms from the bulk are incorporated into the surface layer despite the 20% denser packing. Inspection of Fig. 1 tells us that the number of bonds for the atoms is different on both surfaces: while on

the (1×1) each atom has eight nearest neighbors, the average coordination number in the (5×1) unit cell is $7\frac{2}{3}$ per atom. Reducing $\frac{1}{3}$ of a bond per atom costs the energy $\gamma = (\frac{1}{3})(\frac{1}{6})E_{\text{coh}} = 0.39$ eV/atom, with E_{coh} being the cohesive energy, which is 6.94 eV/atom for Ir. Thus the net gain in energy would be $\Delta\gamma \approx 0.53$ eV/atom by relieving the surface stress upon the $(1 \times 1) \rightarrow (5 \times 1)$ reconstruction.

VI. CONCLUSION

The results and discussion presented above clearly reveal the different dynamical properties of the Ir(100)- (1×1) and Ir(100)- (5×1) surface. In both high symme-

try directions the frequency of the Rayleigh phonon near the zone boundary is higher on the unreconstructed (1×1) surface. A lattice-dynamical analysis shows that this enlarged frequency can be attributed to a strong tensile surface stress. We conclude that this surface stress is the driving force for the $(1 \times 1) \rightarrow (5 \times 1)$ reconstruction of the Ir(100) surface.

ACKNOWLEDGMENTS

One of us (J.G.C.) acknowledges support from the Alexander von Humboldt-Stiftung. The able assistance of D. Bruchmann and U. Marx-Birmans is appreciated.

*Present address: Corporate Research Science Laboratories, Exxon Research and Engineering Company, Annandale, NJ 08801.

¹S. Lehwald, J. Sztetfel, H. Ibach, T. S. Rahman, and D. L. Mills, Phys. Rev. Lett. **50**, 518 (1983).

²J. E. Black, in *Structure and Dynamics of Surfaces*, Vol. I of *Topics in Current Physics*, edited by W. Schommers and P. von Blanckenhagen (Springer-Verlag, Berlin, 1986), p. 153, and references therein.

³S. Lehwald, F. Wolf, H. Ibach, B. M. Hall, and D. L. Mills, Surf. Sci. **192**, 131 (1987), and references therein.

⁴J. Witt and K. Müller, Phys. Rev. Lett. **57**, 1153 (1986); K. Müller, J. Witt, and O. Schütz, J. Vac. Sci. Technol. A **5**, 757 (1987).

⁵K. Heinz, G. Schmidt, L. Hammer, and K. Müller, Phys. Rev. B **32**, 6214 (1985); N. Bickel and K. Heinz, Surf. Sci. **163**, 435 (1985).

⁶J. Küppers and H. Michel, Appl. Surf. Sci. **3**, 179 (1979).

⁷B. Voigtländer, D. Bruchmann, S. Lehwald, and H. Ibach, Surf. Sci. **225**, 151 (1990).

⁸S. Lehwald, M. Rocca, H. Ibach and T. S. Rahman, J. Electron Spectrosc. Relat. Phenom. **38**, 29 (1986).

⁹R. G. Musket, W. McLean, C. A. Colmenares, D. M. Makowiecki, and W. J. Siekhaus, Appl. Surf. Sci. **10**, 143 (1982).

¹⁰T. N. Rhodin and G. Broden, Surf. Sci. **60**, 466 (1976).

¹¹K. Heinz, G. Schmidt, L. Hammer, and K. Müller, Phys. Rev. B **32**, 6214 (1985).

¹²R. E. Allen, G. P. Alldredge, and F. W. de Wette, Phys. Rev. B **4**, 1661 (1971).

¹³M. Rocca, H. Ibach, S. Lehwald, and T. S. Rahman, in *Structure and Dynamics of Surfaces* (Ref. 2), p. 245; M. Rocca, S. Lehwald, H. Ibach, and T. S. Rahman, Surf. Sci. **171**, 632 (1986).

¹⁴M-L. Xu, B. M. Hall, S. Y. Tong, M. Rocca, S. Lehwald, H.

Ibach, and J. Black, Phys. Rev. Lett. **54**, 1171 (1985).

¹⁵J. E. Black, D. L. Mills, W. Daum, C. Stuhlmann, and H. Ibach, Surf. Sci. **217**, 529 (1989).

¹⁶K. E. Kuhnke and K. Kern (unpublished).

¹⁷V. V. Nemoshkaleiko, V. Yu. Mil'man, A. V. Zhalko-Titarenko, V. N. Antonov, and Yu. L. Shitikov, Pis'ma Zh. Eksp. Teor. Fiz. **47**, 245 (1988) [JETP Lett. **47**, 295 (1988)].

¹⁸H. Ibach and T. S. Rahman, in *Chemistry and Physics of Solid Surfaces V*, edited by R. Vanselow and R. Howe (Springer-Verlag, Berlin, 1984).

¹⁹R. E. MacFarlane, J. A. Rayne, and C. K. Jones, Phys. Lett. **20**, 234 (1966).

²⁰D. G. Castner, G. A. Somorjai, J. E. Black, D. Castiel, and R. F. Wallis, Phys. Rev. B **24**, 1616 (1981).

²¹P. H. Dederichs, H. Schober, and D. J. Sellmyer, in *Phonon States of Elements, Electron States and Fermi Surfaces of Alloys*, Vol. 13a of *Landolt-Börnstein*, edited by K.-H. Hellwege and J. L. Olsen (Springer, Berlin, 1981), p. 118.

²²M. Wuttig, R. Franchy, and H. Ibach, Z. Phys. B **65**, 71 (1986).

²³J. S. Nelson, E. C. Sowa, and M. S. Daw, Phys. Rev. Lett. **61**, 1977 (1988).

²⁴J. A. Gaspar and A. G. Eguiluz, Phys. Rev. B **40**, 11976 (1989).

²⁵D. W. Jepsen, P. M. Marcus, and F. Jona, Phys. Rev. B **5**, 3933 (1972).

²⁶B. M. Hall, D. L. Mills, M. H. Mohamed, and L. L. Kesmodel, Phys. Rev. B **38**, 5856 (1988).

²⁷D. C. Gazis, R. Hermans, and R. F. Wallis, Phys. Rev. **119**, 533 (1960).

²⁸M. C. Payne, N. Roberts, and R. J. Needs, Surf. Sci. **211/212**, 1 (1989).

²⁹W. Menezes, P. Knipp, G. Tisdale, and S. J. Sibener, Phys. Rev. B **41**, 5648 (1990).